J|A|C|S
ARTICLES
Published on Web 03/25/2004

Ellipsometric Approach for the Real-Time Detection of Label-Free Protein Adsorption by Second Harmonic Generation

Mark A. Polizzi, Ryan M. Plocinik, and Garth J. Simpson*

Contribution from the Department of Chemistry, Purdue University, 560 Oval Drive, West Lafayette, Indiana 47907

Received December 10, 2003; E-mail: gsimpson@purdue.edu

Abstract: Second harmonic generation (SHG) was performed using a novel ellipsometric detection approach to selectively probe the real-time surface binding kinetics of an unlabeled protein. The coherence of nonlinear optical processes introduces new possibilities for exploiting polarization that are unavailable with incoherent methods, such as absorbance and fluorescence. Adsorption of bovine serum albumin (BSA) at silica/aqueous solution interfaces resulted in changes in the polarization state of the frequency-doubled light through weak, dynamic interactions with a coadsorbed nonlinear optical probe molecule (rhodamine 6G). Using a remarkably simple instrumental approach, signals arising exclusively from surface interactions with BSA were spatially isolated and selectively detected with high signal-to-noise. The relative intensities acquired during the kinetics experiments using both circularly and linearly polarized incident beams were in excellent agreement with the responses predicted from SHG ellipsometry polarization measurements. Analysis of the polarization-dependent SHG generated during BSA adsorption at glass/aqueous solution interfaces provided direct evidence for slow conformational changes within the protein layer after adsorption, consistent with protein denaturation. This polarization selection approach is sufficiently general to be easily extended to virtually all coherent nonlinear optical processes and a variety of different surface interactions and architectures.

Introduction

The surface selectivity of second harmonic generation (SHG) coupled with the reasonably high sensitivity and simple instrumentation requirements suggest significant potential for the use of nonlinear optical methods in biosensing applications. By providing surface-specific information in real time, nonlinear optical sensing approaches present attractive alternatives to other optical-based sensing techniques for in situ detection of unlabeled proteins, including surface plasmon resonance (SPR),[1−5] traditional ellipsometry,[6,7] and waveguide techniques.[7−12] Furthermore, nonlinear optical approaches are largely insensitive to subtle changes in the bulk refractive index that often plague SPR, waveguide, and ellipsometry analyses.[1−3] Most of these linear optical methods also impose specific requirements on the surfaces and/or substrates that can be used. The greater flexibility in substrate selection and inherent surface specificity of surface second harmonic generation has led many groups to pursue nonlinear optical approaches for transducing protein/interface interactions.[13−22] Since methods for reliably detecting unlabeled proteins are far more attractive for a host of practical reasons, the large majority of SHG protein adsorption studies to date have relied on detecting the native nonlinear optical protein response (analogous to autofluorescence).[13−18,21−30] Notable

(1) Kooyman, R. P. H.; de Bruijn, H. E.; Eenink, R. G.; Greve, J. *J. Mol. Struct.* **1990**.
(2) Homola, J.; Yee, S. S.; Gunter, G. *Sens. Actuators B* **1999**, *54*, 3.
(3) Elwing, H. *Biomaterials* **1998**, *19*, 397.
(4) Green, R. J.; Davies, J.; Davies, M. C.; Roberts, C. J.; Tendler, S. J. B. *Biomater.* **1997**, *18*, 405.
(5) Silin, V.; Weetall, H.; Vanderah, D. J. *J. Colloid Interface Sci.* **1997**, *185*, 94.
(6) Krisdhasima, V.; Vinaraphong, P.; McGuire, J. *J. Colloid Interface Sci.* **1993**, *161*, 325.
(7) Höök, F.; Vörös, J.; Rodahl, M.; Kurrat, R.; Böni, P.; Ramsden, J. J.; Textor, M.; Spencer, N. D.; Tengvall, P.; Gold, J.; Kasemo, B. *Colloids Surf. B* **2002**, *24*, 155.
(8) Bradshaw, J. T.; Mendes, S. B.; Saavedra, S. S. *Anal. Chem.* **2002**, *74*, 1751.
(9) Bradshaw, J. T.; Mendes, S. B.; Armstrong, N. R.; Saavedra, S. S. *Anal. Chem.* **2003**, *75*, 1080.
(10) Calonder, C.; Tie, Y.; Van Tassel, P. R. *Proc. Natl. Acad. Sci. U.S.A.* **2001**, *98*, 10664.
(11) Vörös, J.; Ramsden, J. J.; Csucs, G.; Szendro, I.; De Paul, S. M.; Textor, M.; Spencer, N. D. *Biomaterials* **2002**, *23*, 3699.
(12) Brusatori, M. A.; Tie, Y.; Van Tassel, P. R. *Langmuir* **2003**, *19*, 5089.
(13) Eijt, S. W. H.; Wittebrood, M. M.; Devillers, M. A. C.; Rasing, T. *Langmuir* **1994**, *10*, 4498.
(14) Smiley, B. L.; Vogel, V. *J. Chem. Phys.* **1995**, *103*, 3140.
(15) Rinuy, J.; Brevet, P. F.; Girault, H. H. *Biophys. J.* **1999**, *77*, 3350.
(16) Perrenoud-Rinuy, J.; Brevet, P. F.; Girault, H. H. *Phys. Chem. Chem. Phys.* **2002**, *4*, 4774.
(17) Hicks, J. M.; Petralli-Mallow, T. *Appl. Phys. B* **1999**, *68*, 589.
(18) Petralli-Mallow, T.; Plant, A. L.; Lewis, M. L.; Hicks, J. M. *Langmuir* **2000**, *16*, 5960.
(19) Salafsky, J. S. *Chem. Phys. Lett.* **2001**, *342*, 485.
(20) Salafsky, J. S.; Eisenthal, K. B. *J. Phys. Chem. B* **2000**, *104*, 7752.
(21) Kriech, M. A.; Conboy, J. C. *J. Am. Chem. Soc.* **2003**, *125*, 1148.
(22) Conboy, J. C.; Kriech, M. A. *Anal. Chim. Acta* **2003**, *496*, 143.
(23) Clays, K.; Van Elshocht, S.; Chi, M.; Lepoudre, E.; Persoons, A. *J. Opt. Soc. Am. B* **2001**, *18*, 1474.
(24) Campagnola, P. J.; Millard, A. C.; Terasaki, M.; Hoppe, P. E.; Malone, C. J.; Mohler, W. A. *Biophys. J.* **2002**, *81*, 493.
(25) Mohler, M.; Millard, A. C.; Campagnola, P. J. *Methods* **2003**, *29*, 97.
(26) Cox, G.; Kable, E.; Jones, A.; Fraser, I.; Manconi, F.; Gorrell, M. D. *J. Struct. Biol* **2003**, *141*, 53.
(27) Brown, E.; McKee, T.; diTomaso, E.; Pluen, A.; Seed, B.; Boucher, Y.; Jain, R. K. *Nature Med.* **2003**, *9*, 796.

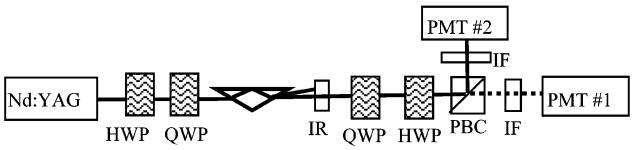

Figure 1. Schematic of the instrumental apparatus. HWP, half-wave plate; QWP, quarter-wave plate; IR, infrared absorbing filter; PBC, polarizing beam splitting cube; IF, 532 nm interference filter. In a NONE polarization measurement, the QWP and HWP following the sample are iteratively rotated until an intensity minimum is recorded at PMT #1. Following this nulling procedure, any light detected at PMT #1 arises exclusively from changes in the surface nonlinear optical response.

exceptions include work by Salafsky, in which protein binding kinetics were measured using "SHG-labels",[19] and by Salafsky and Eisenthal, in which protein binding was transduced from the concomitant reduction in the native background SHG response of the charged silica/water interface.[20]

With the one exception of the study by Salafsky and Eisenthal,[20] a major limitation of these previous nonlinear optical studies has been the required use either of proteins with substantial native nonlinear optical activities or of labeled proteins. Clearly, altering a protein by the attachment of a fluorescent or SHG-active label not only potentially influences its biological and surface activity,[31,32] it also introduces additional sample preparation procedures. Alternatively, reliance on the native protein nonlinear optical response generally prohibits the facile detection of protein−protein interactions using surface-immobilized proteins, for which the SHG-activity of the initial protein-decorated surface is likely to compete with the analyte response. Without this flexibility for surface design, methods relying on the native protein nonlinearity generally are limited to monitoring nonspecific surface-association at relatively simple interfaces. Although the method developed by Salafsky and Eisenthal circumvents the need for significant nonlinear optical activity from the native protein,[20] the relatively weak signals obtained from the bare water/silica interface arise exclusively from changes in the surface potential, which again places significant restrictions on the surface architectures that may be employed.

In the present work, nonlinear optical null ellipsometry for signal isolation (NONE-SI) is demonstrated as a novel and general approach for background-free real-time biosensing of protein/surface interactions. An overview of the approach is depicted in Figure 1. In general, the exigent beam in nonlinear optical surface measurements is elliptically polarized (including linear and circular polarizations as specific subsets). By passing the beam through a quarter-wave plate (QWP) rotated at the appropriate angle, the resulting beam can be transformed from elliptically to linearly polarized. With an appropriate selection of a half-wave plate (HWP) rotation angle, the beam can be completely rejected at a subsequent polarizer. Irrespective of the initial polarization state, a combination of half and quarter-wave plate rotation angles exists that produces zero intensity at the detector. From the waveplate rotation angles resulting in intensity minima, the complete polarization state of the nonlinear optical beam can be determined, which is the basis for nonlinear optical null ellipsometry (NONE).[33] Following this nulling procedure, surface binding of an analyte generally induces a change in the polarization state of the nonlinear optical beam. Consequently, the initial combination of waveplate rotation angles no longer yields zero intensity, but rather results in a signal that scales quadratically with the surface concentration of adsorbate (assuming a second-order nonlinear optical process). This ellipsometric approach was used for the real-time background-free detection of unlabeled bovine serum albumin (BSA) adsorption kinetics at the silica/aqueous solution interface, providing insights into charge reorganization during the adsorption process.

Theory

The fundamental concepts of NONE for characterizing surface nonlinearity have been detailed in other work.[33] If the nonlinear beam from the surface is passed through a quarter-wave plate, a half-wave plate, and a polarizer in series as depicted in Figure 1, the detected field is given by the following equation.[33]

$$\boldsymbol{e}_{\mathrm{PMT\#1}}^{2\omega} = N \begin{bmatrix} 0 & 0 \\ -[\sin(2\Delta^{2\omega}) + i\sin(2\alpha_{\mathrm{H}}^{2\omega})] & \cos(2\Delta^{2\omega}) - i\cos(2\alpha_{\mathrm{H}}^{2\omega}) \end{bmatrix} \begin{bmatrix} e_{\mathrm{p}}^{2\omega} \\ e_{\mathrm{s}}^{2\omega} \end{bmatrix} \quad (1)$$

In eq 1, $\Delta^{2\omega} = \alpha_{\mathrm{H}}{}^{2\omega} - \alpha_{\mathrm{Q}}{}^{2\omega}$, and N is a constant proportional to the surface number density of SHG-active chromophores (assuming identical noninteracting chromophores). For an appropriate combination of $\alpha_{\mathrm{H}}{}^{2\omega}$ and $\alpha_{\mathrm{Q}}{}^{2\omega}$, the detected SHG intensity from the initial background response (species A) can be suppressed at photomultiplier tube (PMT) #1 (and correspondingly maximized at PMT #2, depicted in Figure 1), such that $|e_{\mathrm{PMT\#1}}^{2\omega,\mathrm{A}}| = 0$.[33] Introduction of a new source of nonlinear polarization (species B) yields a net polarization from the interface given by the coherent linear combination of the two fields.

$$e_{\mathrm{PMT\#1}}^{2\omega,\mathrm{A}} = (N_{\mathrm{A}} e_{\mathrm{p}}^{2\omega,\mathrm{A}} + N_{\mathrm{B}} e_{\mathrm{p}}^{2\omega,\mathrm{B}})[\cos(2\Delta^{2\omega}) - i\cos(2\alpha_{\mathrm{H}}^{2\omega})] + (N_{\mathrm{A}} e_{\mathrm{p}}^{2\omega,\mathrm{A}} + N_{\mathrm{B}} e_{\mathrm{s}}^{2\omega,\mathrm{B}})[-\sin(2\Delta^{2\omega}) - i\sin(2\alpha_{\mathrm{H}}^{2\omega})] \quad (2)$$

For a selection of α_{H} and α_{Q} producing zero intensity at PMT #1 from species A alone, the detected field, upon introduction of species B, simplifies to a function solely dependent on the nonlinear optical properties of species B.

$$\boldsymbol{e}_{\mathrm{PMT\#1}}^{2\omega} = N_{\mathrm{B}} \begin{Bmatrix} e_{\mathrm{p}}^{2\omega,\mathrm{B}}[\cos(2\Delta^{2\omega,\mathrm{A}}) - i\cos(2\alpha_{\mathrm{H}}^{2\omega,\mathrm{A}})] \\ + e_{\mathrm{s}}^{2\omega,\mathrm{B}}[-\sin(2\Delta^{2\omega,\mathrm{A}}) + i\sin(2\alpha_{\mathrm{H}}^{2\omega,\mathrm{A}})] \end{Bmatrix} \quad (3)$$

In eq 3, the superscripts indicate the NONE ellipsometric angles yielding null signals at PMT#1 for species A alone (or more generally, the initial background SHG response). An important distinction is made between NONE measurements (which are measurements of the QWP and HWP rotation angles producing intensity minima) and NONE-SI measurements (which are measurements of intensity acquired after first

(28) Zoumi, A.; Yeh, A.; Tromberg, B. J. *Proc. Natl. Acad. Sci. U.S.A.* **2002**, *99*, 11014.
(29) Dombeck, D. A.; Kasischke, K. A.; Vishwasrao, H. D.; Ingelsson, M.; Hyman, B.; Webb, W. W. *Proc. Natl. Acad. Sci. U.S.A.* **2003**, *100*, 7081.
(30) Zipfel, W. R.; Williams, R. M.; Christie, R.; Nikitin, A. Y.; Hyman, B.; Webb, W. W. *Proc. Natl. Acad. Sci. U.S.A.* **2003**, *100*, 7075.
(31) Gajraj, A.; Ofoli, R. Y. *Langmuir* **2000**, *16*, 8085.
(32) Crandall, R. E.; Janatova, J.; Andrade, J. D. *Prepr. Biochem.* **1981**, *11*, 111.
(33) Plocinik, R. M.; Simpson, G. J. *Anal. Chim. Acta* **2003**, *496*, 133.

Table 1. Results of the Experimental NONE Polarization Analysis[a]

		$\alpha_H^{\omega} = -22.5°(-45°)$	$\alpha_H^{\omega} = 22.5°(45°)$	$\alpha_H^{\omega} = 0°$(RCP)	$\alpha_H^{\omega} = 45°$(LCP)
R6G/silica	$\alpha_Q^{2\omega}$	71° (±3°)	17° (±1°)	71° (±2°)	114° (±4°)
	$\alpha_H^{2\omega}$	25° (±2°)	43° (±1°)	51° (±2°)	43.4° (±0.8°)
	ρ	0.28 (±0.09)	−0.25 (±0.03)	0.21 (±0.03)	−0.31 (±0.02)
		+0.42i (±0.07i)	−0.42i (±0.04i)	−0.63i (±0.05i)	+0.59i (±0.07i)
BSA/R6G/silica	$\alpha_Q^{2\omega}$	62.8° (±0.8°)	107° (±1°)	61° (±1°)	14° (±2°)
	$\alpha_H^{2\omega}$	21° (±1°)	64° (±2°)	47° (±2°)	61° (±1°)
	ρ	0.43 (±0.03)	−0.25 (±0.05)	0.29 (±0.02)	−0.22 (±0.05)
		+0.45i (±0.02i)	−0.41i (±0.04i)	−0.74i (±0.08i)	+0.36i (±0.04i)

[a] Values in parentheses indicate one standard deviation from four separate measurements. The incident QWP was fixed at $\alpha_Q^{\omega} = -45°$ for all reported values.

performing a NONE minimization). Using this simple and general polarization selection approach, the detected intensity becomes independent of the number density of species A and scales quadratically with the number density of species B.

$$I_{\mathrm{PMT\#1}}^{2\omega} \propto N_{\mathrm{B}}^2 |e_{\mathrm{PMT\#1}}^{2\omega}|^2 \tag{4}$$

Experimental Section

The SHG measurements were carried out in total internal reflection using a fused silica right-angle prism (ESCO Products, S1−UV). The solutions were introduced to the surface through a flow cell built in house. Prior to each use, the prism was immersed in a bath of chromic acid for 10 min, rinsed with ultrapure water, and dried under a stream of nitrogen. Rhodamine 6G (R6G, Aldrich, ∼95% pure) was used without purification and was solvated in high purity water (resistivity of >17.5 MΩ cm). In each set of kinetics measurements, two solutions were prepared, one with R6G and the other with bovine serum albumin (BSA, Mallinckrodt ∼99.5% pure) and an identical concentration of R6G.

A schematic of the instrument is shown in Figure 1 and described in detail in previous work.[33] In brief, radiation from an Nd:YAG laser (1064 nm, 5−7 ns pulses) was focused onto the surface (∼1 mJ per pulse). The incident beam was prepared in a given polarization state by an appropriate combination of half-wave plate and quarter-wave plate rotation angles, as shown in Figure 1. The second harmonic beam generated at the total internal reflection interface was passed through a second set of quarter- and half-wave plates, a polarizing beam-splitting cube (PBC), and appropriate spectral and spatial filters prior to detection using a photomultiplier tube.

Polarization analysis of the SHG generated both from the aqueous R6G/fused silica interface (R6G/silica) and the interface between fused silica and an aqueous solution containing both R6G and BSA (BSA/R6G/silica) was performed using a nonlinear optical ellipsometric approach developed in this laboratory.[33] In a given NONE polarization measurement, the SHG intensity detected at PMT #1 was minimized by iterative rotation of the QWP and the HWP along the exigent beam path. NONE polarization data were acquired with the QWP along the incident beam path fixed at $\alpha_Q^{\omega} = -45°$ and for HWP rotation angles of $\alpha_H^{\omega} = -22.5°$, 0°, 22.5°, and 45°, corresponding to linearly polarized light oriented at −45°, right circularly polarized light, linearly polarized light oriented at +45°, and left circularly polarized light, respectively. The intensity minima determined from the NONE measurements for each incident polarization state (four separate measurements for each) were used to determine the complex parameter ρ, equal to the ratio of $e_p^{2\omega}/e_s^{2\omega}$ using the following relation, derived from eq 1.[33]

$$\rho = \frac{e_p^{2\omega}}{e_s^{2\omega}} = \frac{\cos(2\Delta^{2\omega}) - i\cos(2\alpha_H^{2\omega})}{\sin(2\Delta^{2\omega}) + i\sin(2\alpha_H^{2\omega})} \tag{5}$$

NONE polarization measurements were acquired for the R6G aqueous solution/fused silica interface prior to introduction of BSA and after ∼1 h of exposure of the surface to BSA. The NONE intensity minima were always at least a factor of 40 smaller than the intensity maxima (simultaneously recorded on PMT #2).

In a given kinetics experiment, a solution of 0.41 mM R6G was introduced to the surface. The second harmonic response measured by PMT #1 was subsequently minimized by iteratively rotating the QWP and HWP along the detection pathway. A solution containing 2×10^{-5} M BSA (also 0.41 mM R6G) was subsequently introduced through the flow cell, and the second harmonic response was monitored from 5 min prior to injection up to 5 h after injection. When recording the long-time kinetics (>15 min), the laser repetition rate was reduced from 20 to 2 Hz. The raw data were normalized using the intensity of the SHG beam detected at PMT #2 from the R6G solution/fused silica interface as an internal reference.

Results and Discussion

NONE polarization measurements were performed to determine the complete polarization state of the nonlinear beam before and after adsorption of BSA, the results of which are summarized in Table 1. The retention of phase information by null ellipsometric polarization characterization provides substantially greater information content than comparable intensity-based polarization analysis approaches, particularly in resonant or near resonant measurements such as these.[33] The experimentally acquired ρ values summarized in Table 1 were combined using the procedure described in the Supporting Information to yield a full suite of complex-valued effective tensor elements, describing the nonlinear optical responses of the surfaces. In turn, these effective $\chi^{(2)}$ tensor elements (compiled in Table 2) were used to predict the complete polarization state of the exigent SHG beam, including full phase information, for a given input polarization state. Using eqs 1 through 4, the predicted intensity of the detected SHG as a function of the rotation angles of the QWP and HWP positioned along the detection pathway were reconstructed for both p-polarized and right circularly polarized incident beams (Figures 2 and 3, respectively) with no adjustable parameters. The curves shown in Figures 2 and 3 are predicted intensity responses derived solely from the experimentally measured null angles summarized in Table 1. The axes in Figures 2 and 3 were chosen to selectively highlight the angle window around the intensity minima for the initial R6G/silica interface (i.e., the null angles expected prior to introduction of BSA).

Inspection of the calculated intensity-dependent responses shown in Figures 2 and 3 provides a convenient graphical depiction of the origin of the detected NONE-SI intensity. Upon introduction of BSA, the polarization state of the nonlinear beam changes, and the QWP and HWP rotation angles yielding intensity minima correspondingly change. The detected signals

Table 2. Summary of Effective $\chi^{(2)}$ Tensor Elements Measured from the NONE Polarization Analysis

	χ_{ssp}	χ_{pss}	χ_{ppp}	χ_{spp}[a]	χ_{psp}[a]
R6G/silica	1	−0.17 (±0.03) + 0.08i (±0.01i)	0.44 (±0.03) + 0.34i (±0.01i)	−0.06 (±0.06) + 0.02i (±0.01i)	−0.01 (±0.05) − 0.02i (±0.05i)
BSA/R6G/silica	1	−0.12 (±0.02) + 0.107i (±0.005i)	0.40 (±0.02) + 0.37i (±0.04i)	−0.16 (±0.05) − 0.19i (±0.01i)	0.07 (±0.03) − 0.06i (±0.03i)

[a] Indicates effective tensor elements that are only expected to be nonzero in chiral films.

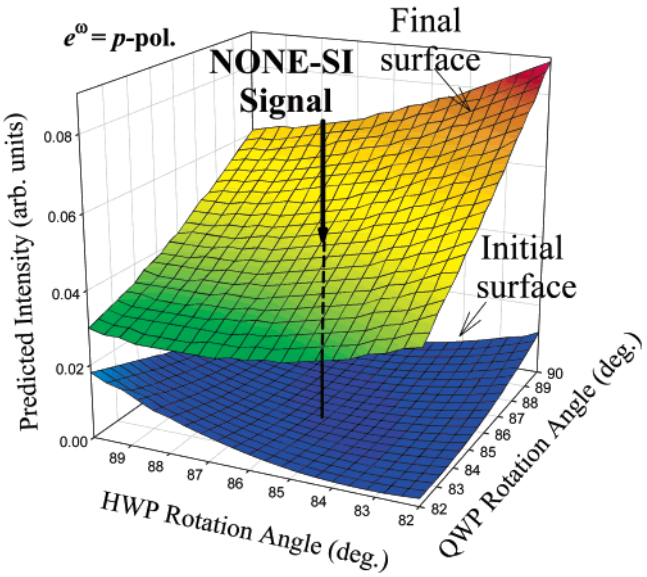

Figure 2. Calculated intensities of the detected SHG beams as functions of the exigent quarter and half-wave plate rotation angles for a p-polarized incident beam. The detected NONE-SI intensity corresponds to the intensity difference between the two surfaces at the minimum of the initial surface. Initial and Final refer to the R6G/silica and BSA/R6G/silica interfaces, respectively. The theoretical intensities were calculated from the NONE polarization measurements summarized in Table 1.

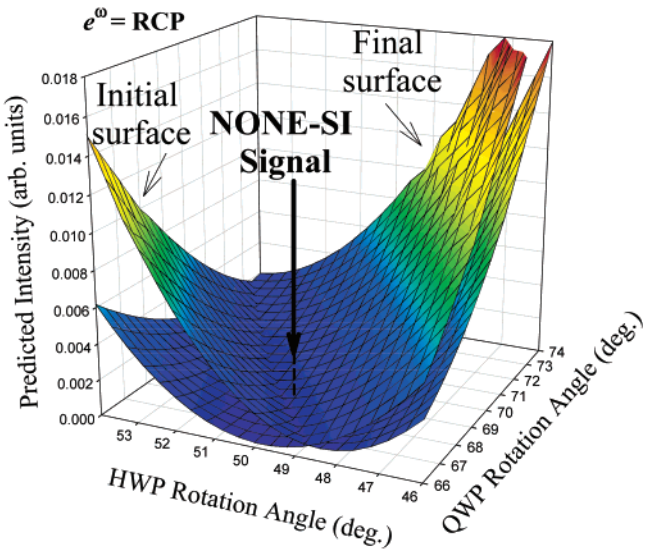

Figure 3. Calculated intensities of the detected SHG beams as functions of the exigent quarter and half-wave plate rotation angles for a right circularly polarized (RCP) incident beam. The detected NONE-SI intensity corresponds to the intensity difference between the two surfaces at the minimum of the initial surface. Initial and Final refer to the R6G/silica and BSA/R6G/silica interfaces, respectively. The theoretical intensities were calculated from the NONE polarization measurements summarized in Table 1.

in the NONE-SI experiments are predicted to scale with the difference between the polarization-dependent relative intensity obtained before and after introduction of BSA (indicated by the solid vertical lines in the figures).

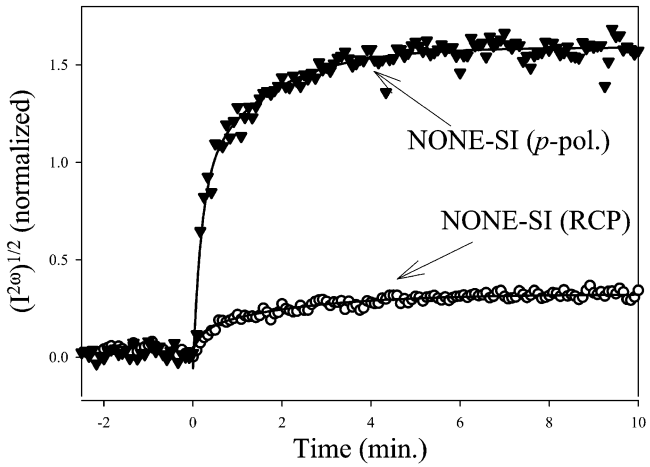

Figure 4. The normalized second harmonic responses for the first 10 min after BSA injection from p-polarized and RCP incident light (open triangles and open circles, respectively). Solid lines are fits of the data to exponential rises to maxima. The NONE-SI (RCP) fit yielded time constant of 4 ± 1 min^{-1}. The NONE-SI (p-polarized) fit yielded a time constant of 5 ± 1 min^{-1}.

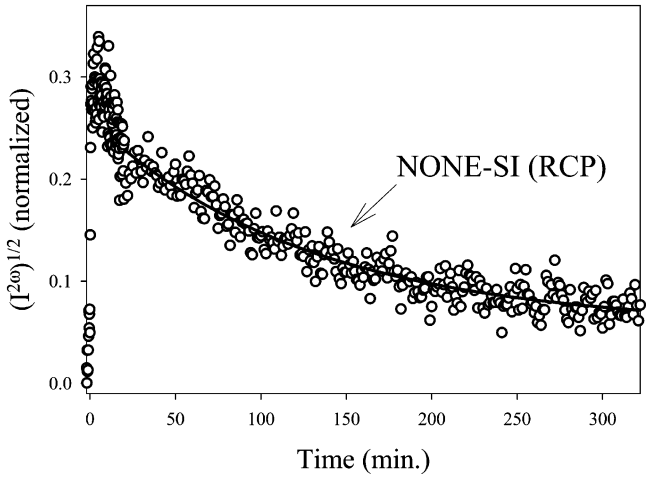

Figure 5. The slow time kinetics of BSA binding to glass is shown. The data were fit to an exponential decay starting at 20 min after the injection of BSA. The fit yielded a time constant of $7.9 \times 10^{-3} \pm 0.5 \times 10^{-3}$ min^{-1}.

Time-dependent kinetics measurements acquired using the NONE-SI method are shown in Figures 4 and 5 upon exposure of the fused silica surface to an aqueous solution containing BSA. Upon introduction of the R6G-BSA solution (time zero), an increase in the measured SHG intensity along both channels was observed. This signal continued to increase for approximately 5 min (Figure 4) before transitioning to a slower decay process that continued for several hours (Figure 5). The solid lines in Figures 4 and 5 are fits of the data to exponential rises to maxima or exponential decays, where appropriate. These trends were reproducible for multiple trials acquired over several days. NONE-SI data were acquired for both right circularly polarized incident light and for p-polarized incident light. In the case of a p-polarized incident beam, a null was obtained for an s-polarized second harmonic beam for the aqueous R6G/

glass interface, consistent with expectations for an achiral surface. In uniaxially oriented systems this latter polarization combination (indicated by I_{sp}) only yields nonzero intensity if the chiral tensor element χ_{YXZ} is nonzero.[34−37] These chiral-specific NONE-SI kinetics measurements indicate a time-dependent increase in SHG-active surface chirality upon exposure to aqueous BSA solutions that mirrors the NONE-SI kinetics responses (also in Figure 4) acquired with circularly polarized incident light.

To assist in interpreting the kinetics measurements shown in Figures 4 and 5, it is helpful to develop a physical model for the origin of the change in the polarization state of the SHG beam upon exposure of the surface to BSA. Several possible mechanisms may be present. For example, BSA itself may be generating SHG with unique polarization characteristics. Certainly, several groups have reported the observations of substantial native SHG from oriented protein assemblies.[13−18,21−30] However, surfaces exposed to BSA alone yielded no detectable SHG under these experimental conditions.[38] Alternatively, previous nonlinear optical studies by Salafsky and Eisenthal have demonstrated that surface binding of protein can substantially alter the surface charge characteristics,[20] which in turn may influence the nonlinear polarization detected using both NONE and NONE-SI. However, this mechanism alone cannot adequately explain the observed increase in the chiral-specific SHG response upon protein binding shown in Figure 4. An alternative and much simpler explanation is that the change in nonlinear polarization arises from rhodamine closely associated with surface-bound protein. It has recently been demonstrated that BSA can act as a chiral template to generate a substantial macroscopic chiral response in SHG arising from chiral orientation of achiral chromophores.[38] Analogous to the chirality present in a propeller comprised of ahiral "blades", chirality within the chromophore is not required in order to generate significant chiroptical effects in the macromolecular surface ensemble. Quantitatively, the macroscopic chiral response from a uniaxially oriented assembly of chromophores of C_{2v} symmetry (or quasi-C_{2v} symmetry as in R6G) is given by the following expression.[39−41]

$$\chi_{XYZ} = \chi_{XZY} = -\chi_{YXZ} = -\chi_{YZX} = \frac{1}{2}N_s\langle \sin^2\theta \sin\psi \cos\psi \rangle (\beta_{x'x'z'} - \beta_{z'x'x'}) \quad (6)$$

Under the resonant conditions used in these investigations, the $\beta_{x'x'z'}$ tensor element dominates the molecular hyperpolarizability of R6G.[33,38,42] Assuming that the molecular hyperpolarizability tensor β_{ijk} for R6G is similar when bound to the surface versus associated with BSA, the greatest difference between species A (R6G at the bare glass/solution interface) and species B (R6G associated with BSA at the glass/solution interface) is the concomitant change in orientation upon interaction with surface-bound BSA. Since the primary biological functions of BSA are the regulation of osmotic pressure and ion transport,[43−46] it is reasonable to suggest the presence of weak but significant interactions between BSA and the charge sites of R6G.[38] Different orientation distributions for the dye molecules are generally expected to produce significantly different nonlinear polarizations. This mechanism is consistent with recent evidence suggesting that orientational effects such as described by eq 6 appear to be the dominant origin of the remarkable sensitivity of SHG to chirality in thin films and interfaces.[47]

Inspection of both the calculated NONE-SI intensities in Figures 2 and 3 and the experimental kinetics measurements in Figure 4 clearly indicates that the magnitude of the NONE-SI response can change significantly when acquired for different polarization states of the incident beam. Using just the NONE polarization measurements compiled in Table 1, the normalized NONE-SI intensities for incident beams of right circularly polarized light compared with p-polarized light are predicted to differ by a factor of 26 (corresponding to a 5.1-fold difference in amplitude). Experimentally, analysis of the data in Figure 4 indicates that the two incident polarization states yield SHG signals that differ by a factor of 5.0 ± 0.3 (averaged from 61 data points acquired between 5 and 10 min), in remarkably good agreement with the theoretical predictions based solely on the measured QWP and HWP null rotation angles compiled in Table 1.

The significantly greater sensitivity observed using NONE-SI with a p-polarized incident beam is intuitively appealing, since this polarization combination (i.e., s-polarized SHG for a p-polarized fundamental beam) selectively probes the chiral-specific SHG response in uniaxial systems.[34−37] Upon exposure to BSA, the surface transitions from achiral to chiral. Consequently, the chiral $\chi^{(2)}$ tensor elements $\chi_{XYZ} = \chi_{XZY} = -\chi_{YXZ} = -\chi_{YZX}$ are zero-valued initially and nonzero after exposure to BSA. The substantial differences in SHG intensity observed using a chiral-specific polarization combination are consistent with this simple physical model.

Irrespective of the specific molecular interactions, the NONE-SI method recovers a simple quadratic scaling behavior between the detected intensity and the number of local perturbations induced by the surface adsorption of BSA. By comparison, this quadratic relationship is not generally maintained in SHG measurements arising from the interference of multiple nonlinear sources.[48,49] In the absence of this background suppression, the intensity can either increase or decrease with increasing analyte number density, with the scaling behavior ranging between linear and quadratic depending on the relative magnitude and phase angle ϕ of the signal and background.[48,49] For example, the

(34) Hicks, J. M.; Petralli-Mallow, T.; Byers, J. D. *Faraday Discuss.* **1994**, *99*, 341.
(35) Byers, J. D.; Yee, H. I.; Hicks, J. M. *J. Chem. Phys.* **1994**, *101*, 6233.
(36) Byers, J. D.; Hicks, J. M. *Chem. Phys. Lett.* **1994**, *231*, 216.
(37) Mazely, T. L.; Hetherington III, W. M. *J. Chem. Phys.* **1987**, *86*, 3640.
(38) Burke, B. J.; Moad, A. J.; Polizzi, M. A.; Simpson, G. J. *J. Am. Chem. Soc.* **2003**, *125*, 9111.
(39) Simpson, G. J. *J. Chem. Phys.* **2002**, *117*, 3398.
(40) Simpson, G. J.; Perry, J. M.; Ashmore-Good, C. L. *Phys. Rev. B* **2002**, *66*, 165437.
(41) Heinz, T. F. Second-Order Nonlinear Optical Effects at Surfaces and Interfaces. In *Nonlinear Surface Electromagnetic Phenomena*; North-Holland: New York, 1991; p 354.
(42) Moad, A. J.; Simpson, G. J. *accepted for publication in J. Phys. Chem. B.*
(43) Voet, D.; Voet, J. G. *Biochemistry*; John Wiley and Sons: New York, 1995.
(44) Foster, J. F. Albumins. In *Albumin structure, function and uses*; Rosenoer, V. M., Oratz, M., Rothschild, M. A., Eds.; Pergamon Press: New York, 1977.
(45) Peters, T. J. Serum Albumin. In *The plasma proteins: structure, function, and genetic control*; Putnam, F. W., Ed.; Academic Press: New York, 1975; Vol. 1.
(46) Brown, J. R.; Shockley, P.; Behrens, P. Q. Albumin: sequence, evolution and structural models. In *The chemistry and physiology of the human plasma proteins*; Bing, D. H., Ed.; Pergamon Press: New York, 1979.
(47) Perry, J. M.; Moad, A. J.; Simpson, G. J., submitted to *J. Phys. Chem. B.*
(48) Dadap, J. I.; Shan, J.; Weling, A. S.; Misewich, J. A.; Heinz, T. F. *Appl. Phys. B* **1999**, *68*, 333.
(49) Nahata, A.; Heinz, T. F. *Opt. Lett.* **1998**, *23*, 67.

intensity detected by PMT #2 $I^{2\gamma}_{\mathrm{PMT\#2}}$ during the kinetics measurements (not shown) contains contributions from both the native surface (species A) and from R6G closely associated with surface-immobilized BSA (species B) as seen below.[48,49]

$$I^{2\omega}_{\mathrm{PMT\#2}} \propto N_{\mathrm{A}}^2|e^{2\omega,\mathrm{A}}|^2 + N_{\mathrm{B}}^2|e^{2\omega,\mathrm{B}}|^2 + 2N_{\mathrm{A}}N_{\mathrm{B}}|e^{2\omega,\mathrm{A}}||e^{2\omega,\mathrm{B}}|\cos\phi \quad (7)$$

In general, the scaling behavior of the detected intensity with surface concentration cannot be unambiguously identified in the presence of a significant background response unless the relative phase angle ϕ is known a priori. If both nonlinear responses arise from different orientation distributions of the same chromophore (as in these investigations), ϕ can be expected to be close to either 0 or π (positive or negative interference), leading to scaling that is linear with the surface concentration at low coverage (in which case the $2N_{\mathrm{A}}N_{\mathrm{B}}|e^{2\omega,\mathrm{A}}||e^{2\omega,\mathrm{B}}|\cos\phi$ term dominates) and approaches quadratic behavior at higher surface coverages (for which $N_{\mathrm{B}}^2|e^{2\omega,\mathrm{B}}|^2$ dominates). By removal of the background response, the intensity detected by PMT #1 using the NONE-SI method recovers a simple quadratic scaling behavior with the surface concentration of species B, irrespective of both the phase angle ϕ and the amplitude of the response from species A.

The kinetic data acquired by the NONE-SI method reveal some interesting trends when compared with previous measurements of BSA binding kinetics at glass/aqueous solution interfaces.[50−53] Previous publications have identified at least two distinct kinetic regimes for BSA adsorption to glass.[50−53] The initial rapid adsorption occurs on the scale of seconds to minutes. Then a slower adsorption process occurs over several hours, which has been attributed to slow reorganization to a more stable surface conformation that minimizes electrostatic repulsions.[50,51,54] On the basis of these previous studies, the amount of BSA at the surface is increasing during the long-time kinetic process shown in Figure 5.[50,51] However, the detected SHG intensity is decreasing, which can be attributed to changes in the availability of the charge sites able to bind R6G during the slow protein reorganization. This slow restructuring is particularly important physiologically. Serum albumins are among the most prolific proteins within the body and are among the first proteins to bind to the surfaces of medical implants.[52,55,56] A layer of surface-bound serum albumin in its native conformational state can produce a surface with high biocompatibility.[52,55,57,58] In contrast, a surface coating of denatured serum albumin can substantially change the cellular response.[52,58] By nature of this bimodal behavior, the biocompatability of implanted devices depends critically on the nature of the serum albumin-surface interactions.[52,58] The overall loss of SHG with time in the long-time kinetic regime shown in Figure 5 indicates a reduction in the number and/or structural order of the cation binding sites, providing evidence supporting the denaturation of the protein at the interface. By comparison, traditional binding measurement techniques of unlabeled proteins such as SPR and ellipsometry only provide information on the average density of surface protein and are largely blind to protein conformation and activity.

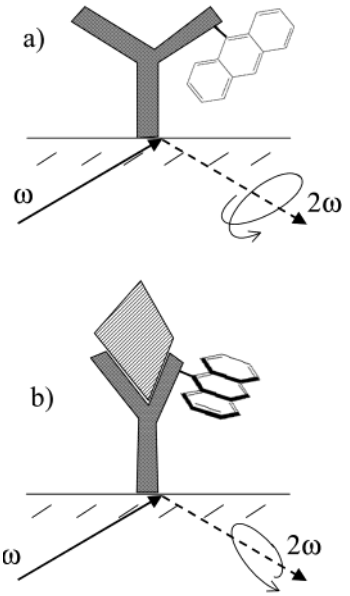

Figure 6. The NONE-SI method can be adapted for measuring specific binding interactions of unlabeled proteins in real time from binding-induced changes in the orientation of an SHG-labeled receptor protein. In part a, the SHG-label on a surface-immobilized antibody is in some initial orientation. Upon binding of the ligand in part b, the concomitant structural reorganization of the protein will generally result in a change in the chromophore orientation distribution and a nonzero NONE-SI signal.

In the present work, weak interactions between the surface and a nonlinear optical probe molecule in dynamic equilibrium were used for monitoring nonspecific protein adsorption at a dielectric interface. However, the generality of NONE-SI extends well beyond selectively probing the emergence of surface chirality using the I_{sp} polarization combination. All that is required for generation of a detected response in NONE-SI is a change in the surface nonlinear polarization (e.g., from changes in the orientation distribution and/or changes in the molecular hyperpolarizability). As one example, a strategy for implementing NONE-SI for selective measurements of specific protein−protein binding interactions is shown schematically in Figure 6. The initial surface consists of an SHG-active probe molecule bound to a surface-immobilized receptor protein (Figure 6a). Irrespective of the initial nonlinear polarizability of the interface, an appropriate combination of waveplates can be found to completely suppress the SHG response detected at PMT #1. Binding of the analyte protein will generally result in a change in the orientation distribution of the SHG-active label (Figure 6b), with a corresponding change in the nonlinear polarization. This change in turn will result in incomplete rejection of the SHG by the waveplates and a detected intensity that scales quadratically with the number of binding events. Consequently, the same basic NONE-SI strategy employed in

(50) Krisdhasima, V.; Vinaraphong, P.; McGuire, J. *J. Colloid Interface Sci.* **1993**, *161*, 325.
(51) Lee, S. H.; Ruckenstein, E. *J. Colloid Interface Sci.* **1988**, *125*, 365.
(52) *Biomaterials: Interfacial phenomena and applications*; Cooper, S. L.; Peppas, N. A., Eds.; American Chemical Society: Washington, DC, 1982; Vol. 199.
(53) Andrade, J. D. Chromatographic analysis of protein adsorption. In *Surface and interfacial aspects of biomedical polymers*; Andrade, J. D., Ed.; Plenum Press: New York, 1985; Vol. 2.
(54) Cheng, Y.-L.; Lok, B. K.; Roberston, C. R. Interactions of macromolecules with surfaces in shear fileds using visible wavelength total internal reflection fluorescence. In *Surface and interfacial aspects of biomedical polymers*; Andrade, J. D., Ed.; Plenum Press: New York, 1985; Vol. 2.
(55) Silverberg, A. Modeling of protein adsorption. In *Surface and interfacial aspects of biomedical polymers*; Andrade, J. D., Ed.; Plenum Press: New York, 1985; Vol. 2.
(56) Kasemo, B. *Solid State Mater. Sci.* **1998**, *3*, 451.
(57) Absolom, D. R. Erythrocyte adhesion to polymer surfaces: Physicochemical and hydrodynamic factors. In *Surface Characterization of Biomaterials*; Ratner, B., D., Ed.; Elsevier: New York, 1988; Vol. 6; p 235.
(58) Shen, M.; Horbett, T. A. *J. Biomed. Mater. Res.* **2001**, *57*, 336.

the present nonspecific binding studies is expected to be equally applicable in label-free real-time measurements of specific protein−protein binding interactions.

The remarkable sensitivity of the nonlinear polarization to subtle changes in surface structure and orientation demonstrated in this work suggests that NONE-SI has the potential to be applicable for background suppression and signal isolation in virtually all nonlinear optical techniques, including sum-frequency generation (SFG), coherent anti-Stokes Raman (CARS) spectroscopies, and degenerate four-wave mixing (D4WM).

Acknowledgment. The authors gratefully acknowledge financial support from a Camille and Henry Dreyfus New Faculty Award, a Research Corporation Research Innovation Award, Purdue University, and the National Science Foundation (CHE-0316177).

Supporting Information Available: The mathematical approach used to generate the predicted SHG intensities in Figures 2 and 3 from the measured NONE angles summarized in Table 1. This material is available free of charge via the Internet at http://pubs.acs.org.

JA031627V